Naval Research Laboratory
Washington, DC 20375-5320

NRL/MR/5328--05-8877

Results of July 2003 Space-Time Delta-Sigma Hardware Experiments at China Lake

Dan P. Scholnik
Jeffrey O. Coleman
Josef Brandriss

Advanced Radar Systems Branch
Radar Division

Donald Bowling
Michael Neel
Scot Rogala
Frank Schiavone

Naval Air Warfare Division
China Lake, CA

September 26, 2005

REPORT DOCUMENTATION PAGE

Form Approved
OMB No. 0704-0188

1. REPORT DATE *(DD-MM-YYYY)*	2. REPORT TYPE	3. DATES COVERED *(From - To)*
26-09-2005	Memorandum Report	

4. TITLE AND SUBTITLE

Results of July 2003 Space-Time Delta-Sigma Hardware Experiments at China Lake

5a. CONTRACT NUMBER

5b. GRANT NUMBER

5c. PROGRAM ELEMENT NUMBER

6. AUTHOR(S)

Dan P. Scholnik, Jeffrey O. Coleman, Josef Brandriss, Donald Bowling,* Michael Neel,* Scot Rogala,*and Frank Schiavone*

5d. PROJECT NUMBER

5e. TASK NUMBER

5f. WORK UNIT NUMBER

7. PERFORMING ORGANIZATION NAME(S) AND ADDRESS(ES)

Naval Research Laboratory, Code 5328
4555 Overlook Avenue, SW
Washington, DC 20375-5320

8. PERFORMING ORGANIZATION REPORT NUMBER

NRL/MR/5328--05-8877

9. SPONSORING / MONITORING AGENCY NAME(S) AND ADDRESS(ES)

10. SPONSOR / MONITOR'S ACRONYM(S)

11. SPONSOR / MONITOR'S REPORT NUMBER(S)

12. DISTRIBUTION / AVAILABILITY STATEMENT

Approved for public release; distribution is unlimited.

13. SUPPLEMENTARY NOTES

*Naval Air Warfare Center, China Lake, CA

14. ABSTRACT

This report presents an overview of the test setup, procedures, and important results from the July 2003 experiments. It does not document an operational or prototype system, provide any mathematical background (references are provided), or contain sufficient detail to recreate the experiments.

15. SUBJECT TERMS

Space-time; Delta-Sigma; Sigma-Delta; Wideband arrays; Digital beamforming

16. SECURITY CLASSIFICATION OF:			17. LIMITATION OF ABSTRACT	18. NUMBER OF PAGES	19a. NAME OF RESPONSIBLE PERSON
a. REPORT	b. ABSTRACT	c. THIS PAGE			Dan P. Scholnik
Unclassified	Unclassified	Unclassified	UL	14	19b. TELEPHONE NUMBER *(include area code)* (202) 404-1943

Standard Form 298 (Rev. 8-98)
Prescribed by ANSI Std. Z39.18

CONTENTS

Results of July 2003 Space-Time Delta-Sigma Hardware Experiments at China Lake

Dan P. Scholnik, Jeffrey O. Coleman and Josef Brandriss
Radar Division, Naval Research Laboratory
Washington, DC
Email: scholnik@nrl.navy.mil, jeffc@radar.nrl.navy.mil

Donald Bowling, Michael Neel, Scot Rogala, and Frank Schiavone
Naval Air Warfare Center
China Lake, CA

Scope: This report presents an overview of the test setup, procedures, and important results from the July 2003 experiments. It does not document an operational or prototype system, provide any mathematical background (references are provided), or contain sufficient detail to recreate the experiment.

I. Executive Summary

Spatio-temporal delta-sigma ($\Delta\Sigma$) modulation, a concept developed at NRL, is an extension of conventional $\Delta\Sigma$ modulation to signals that are functions of space as well as time. At the current time the primary research focus is on its use in transmit antenna arrays, where each antenna element is driven by one or more high-power switches and quantization noise is suppressed via noise shaping for propagating spatial frequencies in a temporal frequency band of interest. It is hoped that eventually the technique will lead to reasonably efficient high-power transmit arrays with the extraordinary linearities demanded by future multifunction RF systems. References [1]–[3] provide the mathematical foundation and explore some of the design issues.

In July 2003 the authors spent two weeks performing hardware experiments at the Naval Air Warfare Center in China Lake, CA. The primary goal was to demonstrate the ability to shape the quantization noise of a transmit array in both spatial and temporal frequency. A secondary goal was to show the flexibility of a simple array driven by binary signals by transmitting multiple signals on independent beams and frequencies. The experiments were designed to be both expedient and cost-effective, and as a result the level of performance achieved falls far short of practical system requirements. This did not prevent us from accomplishing our goals, however, and it provided clear directions for the substantial future hardware research and development that will be required for practical implementations.

In the experiments, a six element dual half-loop linear array was driven by amplified digital logic signals that had been spatio-temporally $\Delta\Sigma$-modulated offline, and the resulting far-field spectrum was captured as a function of angle using a programmable pedestal and spectrum analyzer. The element spacing of the array was approximately $\lambda/12$ at the nominal operating frequency of 200 MHz, for a spatial oversampling ratio (OSR) of 6. The sampling rate of 720 MHz and nominal bandwidth of 200 MHz resulted in a temporal OSR of 1.8. Due to the poor attainable SNR the testing was concentrated on this relatively high bandwidth rather than lowering it to improve the temporal OSR. Fig. 1 illustrates the hardware on the transmit side of the experiment, Fig. 2 shows the array geometry, and Figs. 3–7 show the test setup. Tests performed include measuring the drivers and element patterns and calibrating the array (Figs. 8–10), transmitting multiple beams in two Nyquist zones (Figs. 10(e) and 10(f)), transmitting spatio-temporal $\Delta\Sigma$ modulated signals (Figs. 11 and 12), and transmitting "conventional" $\Delta\Sigma$-modulated signals (Fig. 11(c)) for comparison purposes.

This work was supported by the Office of Naval Research.
Manuscript approved December 14, 2005.

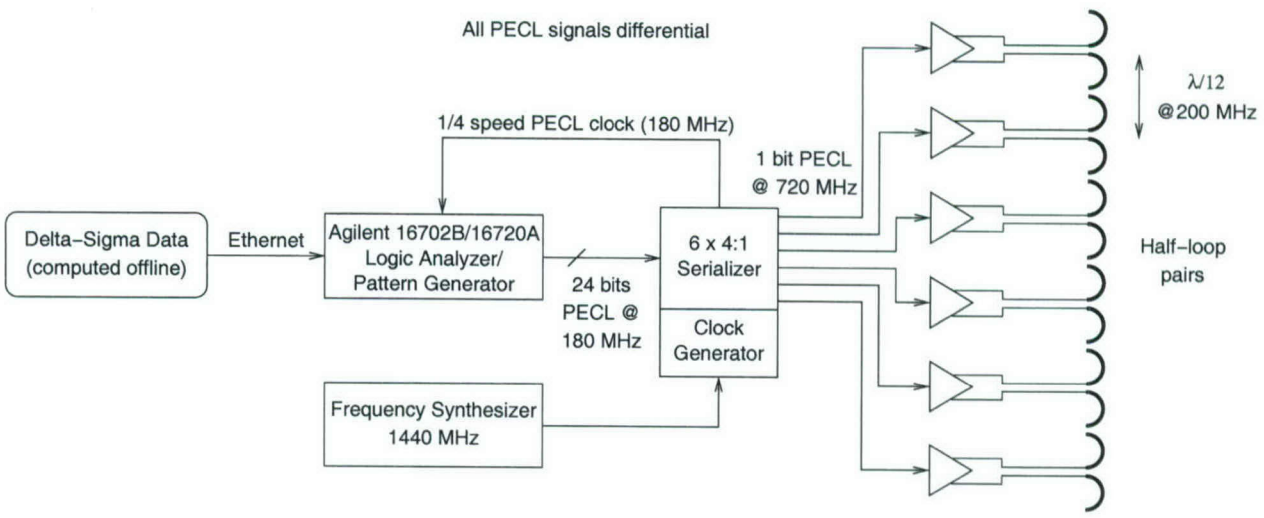

Fig. 1. Transmit-side hardware setup used in experiments.

II. Test Setup

The transmit side of the test setup used for most of the experiments is shown in Fig. 1. The major sections are highlighted below.

A. Digital Signal Generation

Digital waveforms were generated offline using Matlab-based software developed at NRL. These were then uploaded to an Agilent pattern generator over ethernet. Since the pattern generator was placed on top of the antenna pedestal, it was controlled remotely via a web interface. The pattern generator can store up to 16M 24-bit words, and can output them at up to 300 MW/s in a number of different logic formats. We used 24 bit differential PECL outputs at 180 MHz to drive six 4:1 serializers on a custom board, which then output six 720 MHz PECL bit streams. A master 1440 MHz clock was conditioned and divided down as necessary on the board to clock the serializers and pattern generator. The six differential bitstreams were amplified by a pair of AC-coupled op-amps which in turn drove the array elements.

B. Element Drivers

The PECL signals from the serializer board were amplified using a two op-amp circuit. The output of each op-amp was essentially a low-impedance voltage source. These outputs were each connected through a 10Ω current-limiting resistor to the half loops in the array. The other end of each half-loop was grounded. No attempt was made to balance the circuit, thus a high degree of waveform symmetry was not expected. In addition, the driver was not designed with inductive loads in mind. These factors contributed to the relatively poor performance seen in the results.

C. Transmit Array

The transmit array was made up of pairs of square half-loops as shown in Figures 2 and 3. Six pairs made up the active part of the array, with a guard element on each end. The elements were mounted on a 48" by 48" ground plane. The array was designed to be operated at 200 MHz, with approximately six-times spatial oversampling. At this frequency the elements are electrically small, and show little mutual coupling. The impedance of the elements at 200 MHz is approximately $0.5+j50\Omega$, and over a reasonably wide frequency range the elements can be modeled by a 0.5Ω resistor in series with a 40 nH inductor.

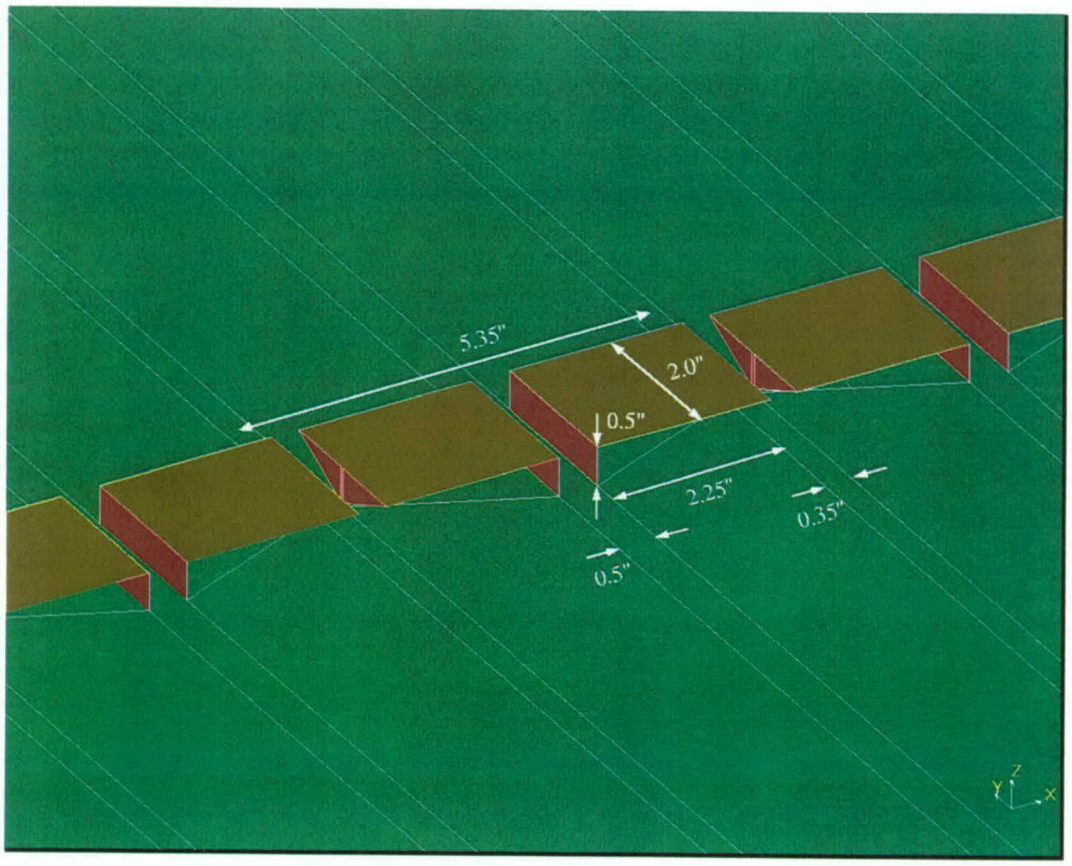

Fig. 2. The spatially oversampled dual half-loop array geometry.

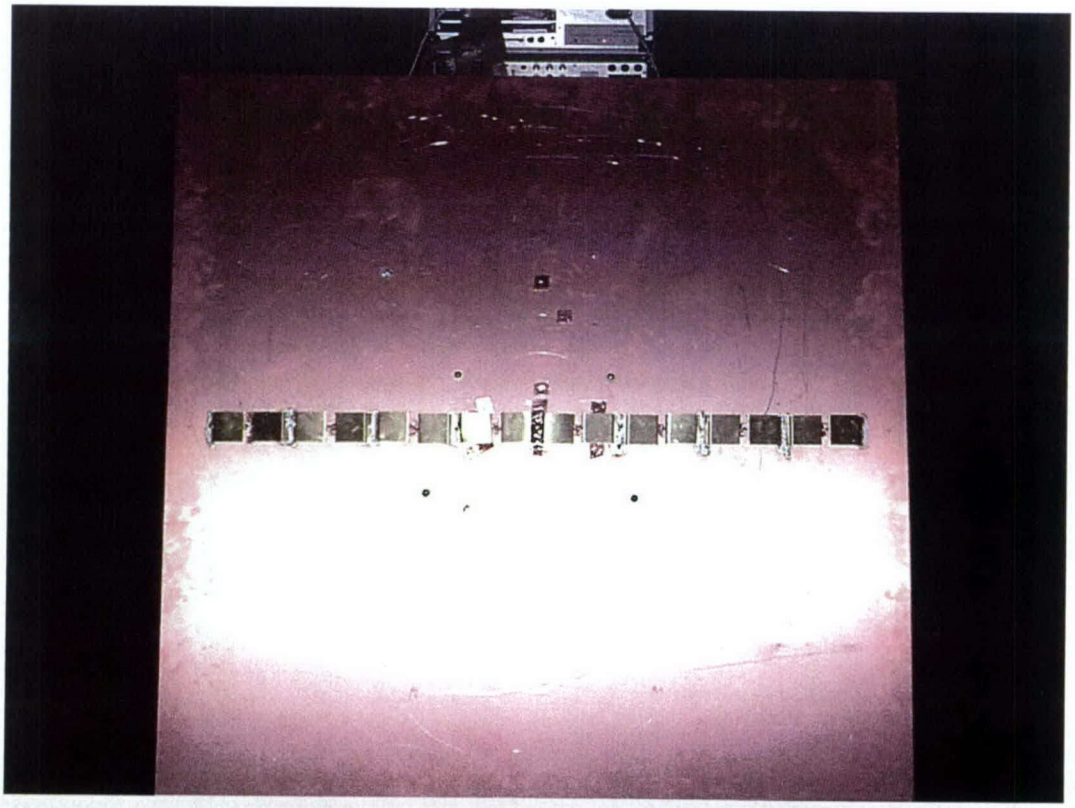

Fig. 3. The array face.

D. Receiver and Antenna

The receive test setup was made as simple as possible: a low-gain (2.5 dB) biconical dipole antenna (shown in Fig. 4) in the far field feeding an LNA, a variable attenuator, another amplifier, and an HP spectrum analyzer. Data was read off of the spectrum analyzer via GPIB using Matlab's Instrument Control Toolbox. The amplifiers were required because the received signal power was, in most cases, too close to the analyzer's noise floor for useful measurements. Additionally the received signal power was in some cases too close to the thermal noise floor to make accurate measurements. We were unable to correct this, as it would have required redesigning the elements, drivers, or both.

E. Pedestal and Control

The array, drivers, serializer board, pattern generator, frequency synthesizer, and power supplies were all mounted on the pedestal in the anechoic chamber, as shown in Figures 5 and 6. Pedestal elevation and azimuth were controlled via GPIB using Matlab's Instrument Control Toolbox. The pedestal controller, various control computers, and the spectrum analyzer were all operated from the control room adjacent to the chamber (Fig. 7).

III. Results

A. Single Channel Tests

We performed single-channel tests to establish a baseline for performance to measure the other tests against. A conventional $\Delta\Sigma$ waveform with a single 200 MHz sinusoid in a 2 MHz noise notch was designed at a sample rate of 240 MHz. Two zeros were then placed between each sample to create a 720 MHz return-to-zero (RZ) waveform with a 33% duty cycle. An RZ waveform was used because it is largely immune to pulse shape asymmetry. The waveform was loaded into the memory for one of the end elements and the resulting output was captured at three points in the system: directly out of the serializer, at the output of the driver, and in the far field. When capturing the serializer and driver outputs they were first disconnected from the downstream components, and only one side of the differential signal was captured. The resulting power spectra are shown in Fig. 8(a), normalized to the peak signal. We can see that while the unloaded driver output is only about 3 dB worse than the serializer output, the radiated and received signal is much worse, by roughly 27 dB. In addition, it shows spurious components not found in the others.

For insight into why the single channel radiated performance is so poor, we used a sampling oscilloscope to measure the driver voltage and current waveforms under load. We used a 11.25 MHz square wave test input and recorded the voltages at the driver output and at the element input. The difference between the two is the voltage across the limiting resistor and thus is proportional to the current flowing though the element. These are shown in Fig. 8(b). We observed a classic RL response with a time constant of about 4 ns (corresponding to 10Ω and 40nH), which is much greater than the 1.39 ns sample time of the 720 MHz data clock. In addition, the waveforms also show considerable ringing that lasts for many fast-clock periods. Neither is necessarily a problem if the underlying mechanism is linear, but we suspect that the driver may not act completely linearly under the inductive load of the element. After a switch the driver is briefly forced to sink current and thus consume power, rather than produce it. We were unable to quantify the linearity of the source of the ripples in the loaded driver in the time allotted.

So, without having the chance to rigorously study the problem, we conclude that there are three likely candidates for the poor performance seen in a single radiated channel. One is nonlinear processes in the driver affecting pulse shape. Another is pulse asymmetry, since the time constant was so long that the RZ waveform would not remove the resulting nonlinear intersymbol interference. A third possibility is interference from the system itself, particularly the digital portions. The small amplitude of the transmitted signal made the system particularly sensitive to such interference.

B. Power, Array Pattern, and Frequency-Response Measurement

A series of measurements were taken to determine the angular and frequency responses of the array and to calibrate power levels. This was done both to aid in simulating the system and to find any obvious problems with the setup.

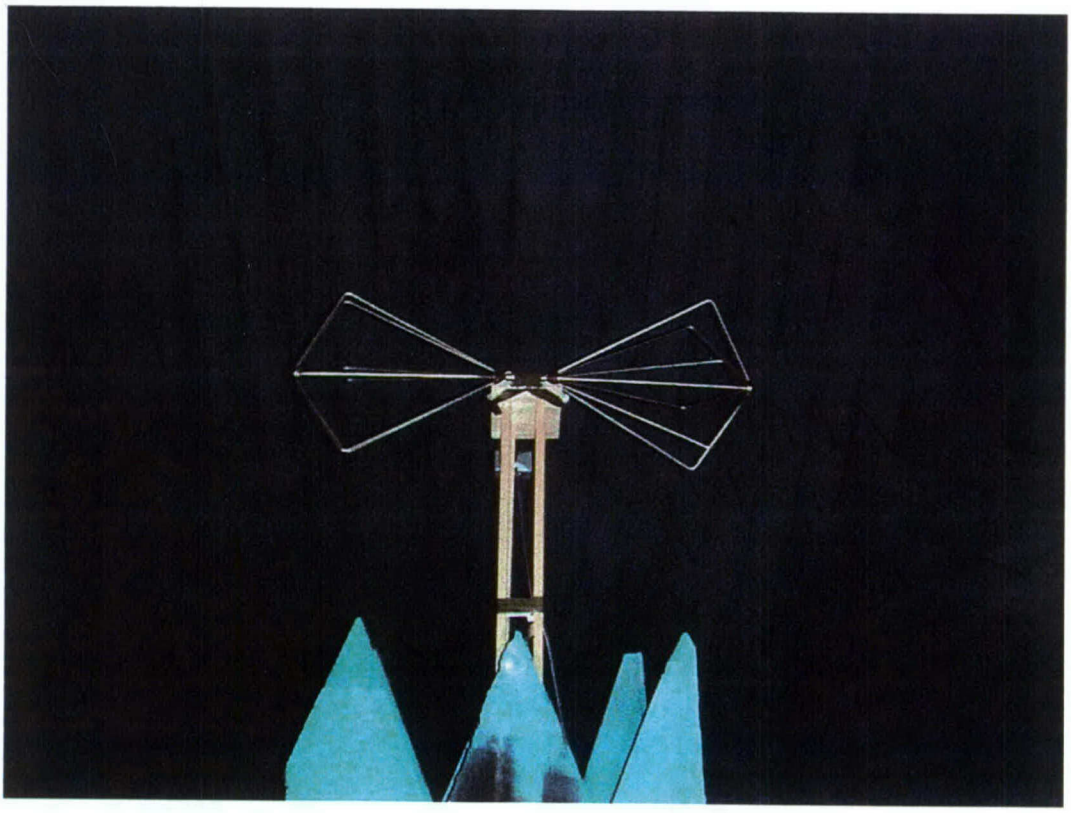

Fig. 4. The biconical receive antenna.

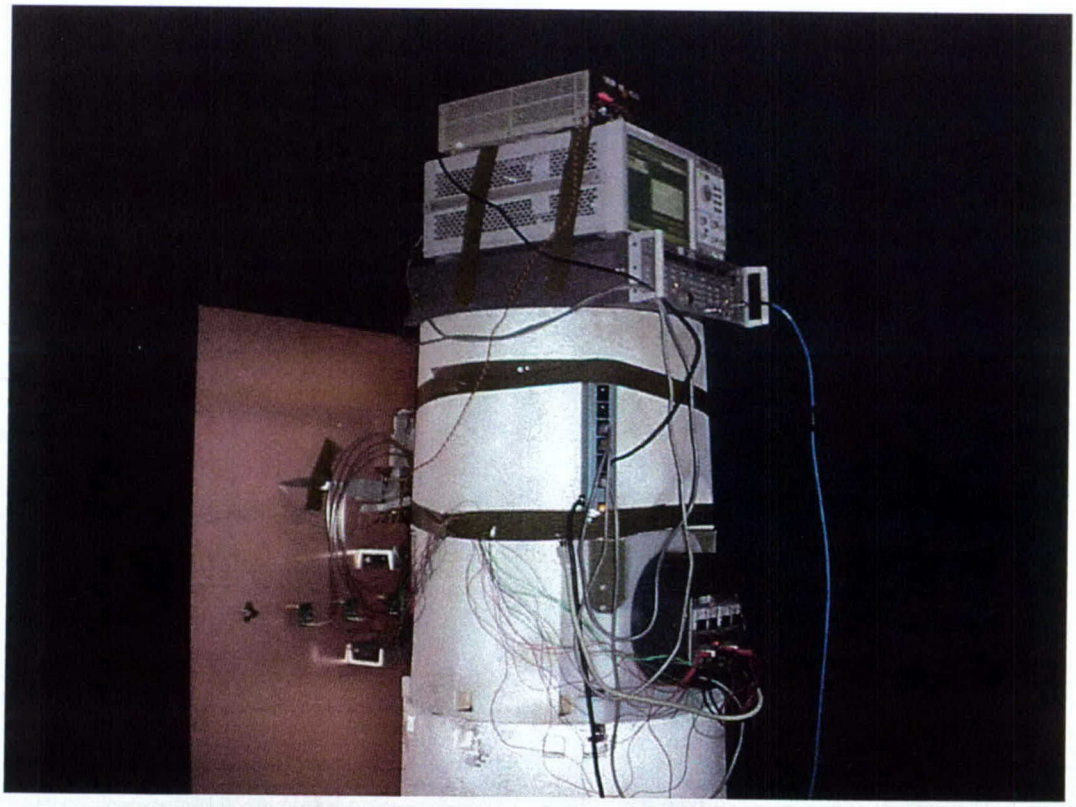

Fig. 5. Hardware setup behind the face

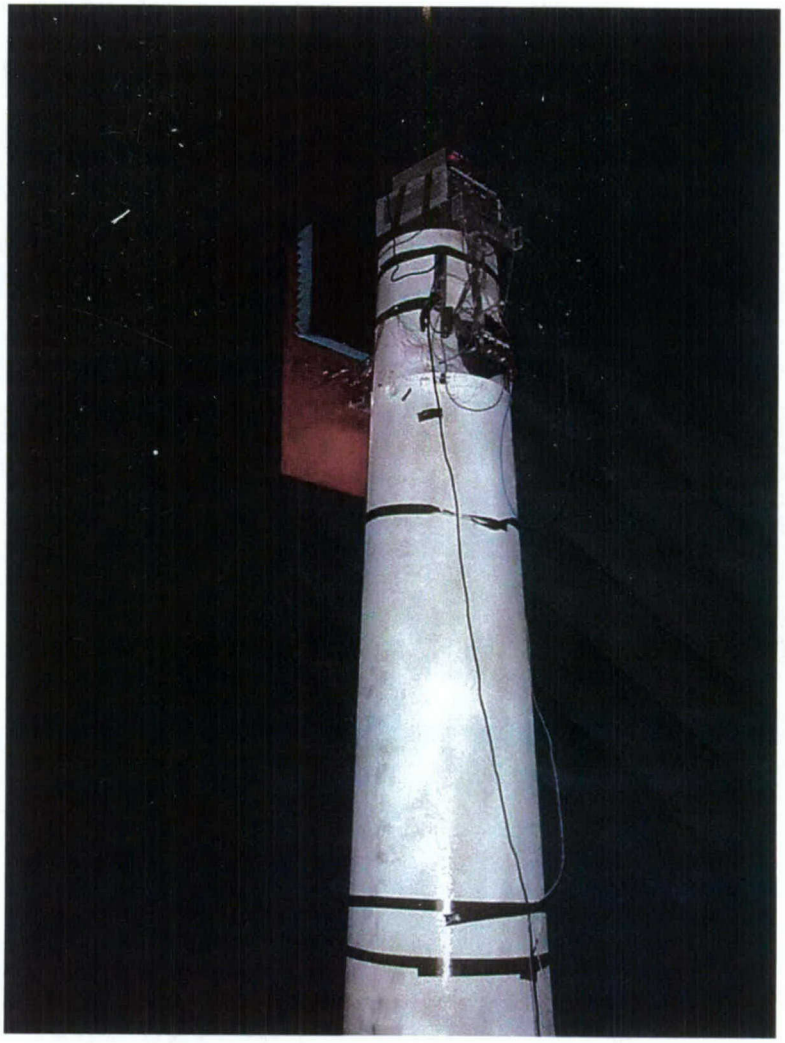

Fig. 6. The array on the pedestal, fully elevated.

Fig. 7. The range control room.

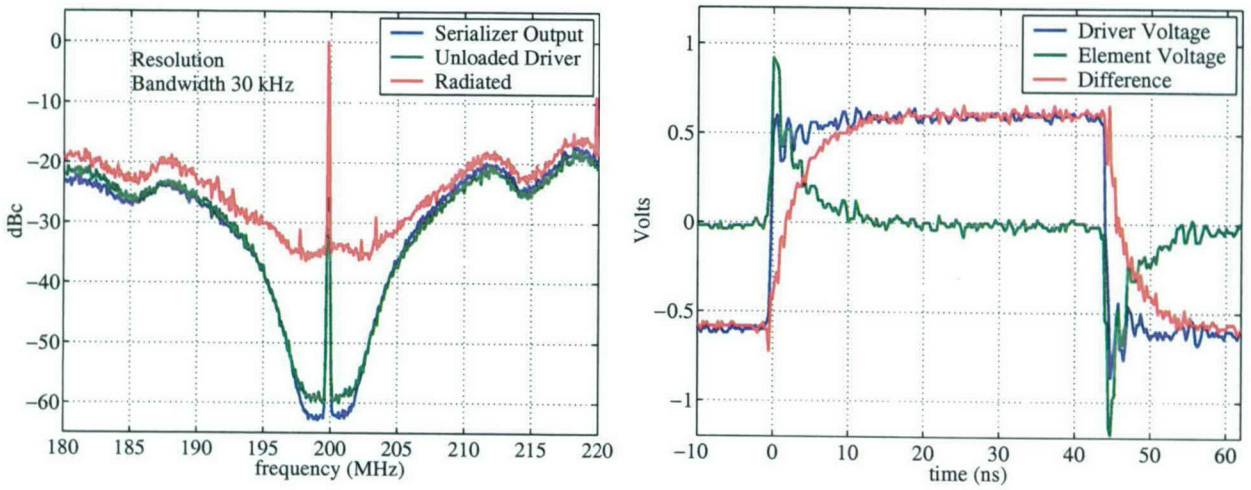

(a) Power spectra due to a single-channel RZ delta-sigma input

(b) Voltages seen at the driver output and element input

Fig. 8. Single channel measurements in frequency and time.

1) Power Levels: The receive antenna was always pointed directly at the array, so we need only account for its frequency response at boresight. This was measured prior to these experiments and is shown in Fig. 9(a). Using this and known propagation and cable losses of 35.5 dB, we then computed the transmitted power in the fundamental of a 180 MHz square wave and a 200 MHz $\Delta\Sigma$-modulated sinusoid as approximately -4.3 dBm and -14.0 dBm, respectively. Assuming equal contributions from each element, this corresponds to approximately -12.1 dBm and -21.8 dBm per element. The modulated sinusoid had an amplitude half that of the square wave, so we expected the power ratio of the two waveforms to be $(4/\pi)^2/0.25 = 8.1$ dB. The slightly higher ratio can be mostly explained due to the transmit array frequency response. These power numbers demonstrate one of the fundamental problems with our setup: a lack of transmit power. For a $\Delta\Sigma$-modulated sinusoid with (say) 100 dB SNR across a 1 MHz band, the noise spectral density will be -160 dBc/Hz. Here this results in a $\Delta\Sigma$ noise floor at the receive antenna of -209.5 dBm/Hz, well below the thermal noise floor. In the end we were forced to settle on a maximum SNR of about 20 dB across a 200 MHz bandwidth, so that the $\Delta\Sigma$ noise floor of approximately -153 dBm/Hz is clearly visible over thermal noise. Since this was still less than the minimum noise floor of the spectrum analyzer (about -150 dBm/Hz), we had to use the aforementioned amplifier chain. These low power levels (and poor digital circuit shielding) help explain why interference was a substantial problem. Referring back to Fig. 8(a), we see that the measured noise floor of the received signal is approximately -140 dBm/Hz (using the RZ waveform reduces the amplitude by about 10 dB). This gives a rough idea of the level of interference and the lowest measurable noise floors.

2) Frequency Responses: To find the transmit array frequency response, we transmitted a $\Delta\Sigma$-modulated multitone signal, containing equal height sinusoids with frequencies spaced at 25 MHz intervals from 25 MHz to 350 MHz. Due to aliasing, this waveform effectively covers an infinite range of frequencies. By calibrating out the frequency responses of the $\Delta\Sigma$ modulator, driver pulse shaping, and the receive array, we computed the transmit frequency response, shown in Fig. 9(b) normalized to the gain at our nominal operating frequency of 200 MHz. Overall the trend is an increase of gain with frequency, with some leveling off at lower frequencies. Note that the gain difference between 180 MHz and 200 MHz is approximately the 2 dB difference seen when performing the power calibration.

3) Array Patterns and Multiple Beams: The measured element patterns at 200 MHz are shown in Fig. 10(a), normalized to a unity peak gain. Clearly the elements do not have identical patterns, although opposing pairs do show a high level of symmetry around boresight. Although we used guard elements and the elements are nominally electrically small and free of mutual coupling, there is some coupling seen in electromagnetic simulations of the array. Perhaps a larger effect, however, is the relatively small size of the ground plane, and the varying distances from the elements to the edge. In future experiments

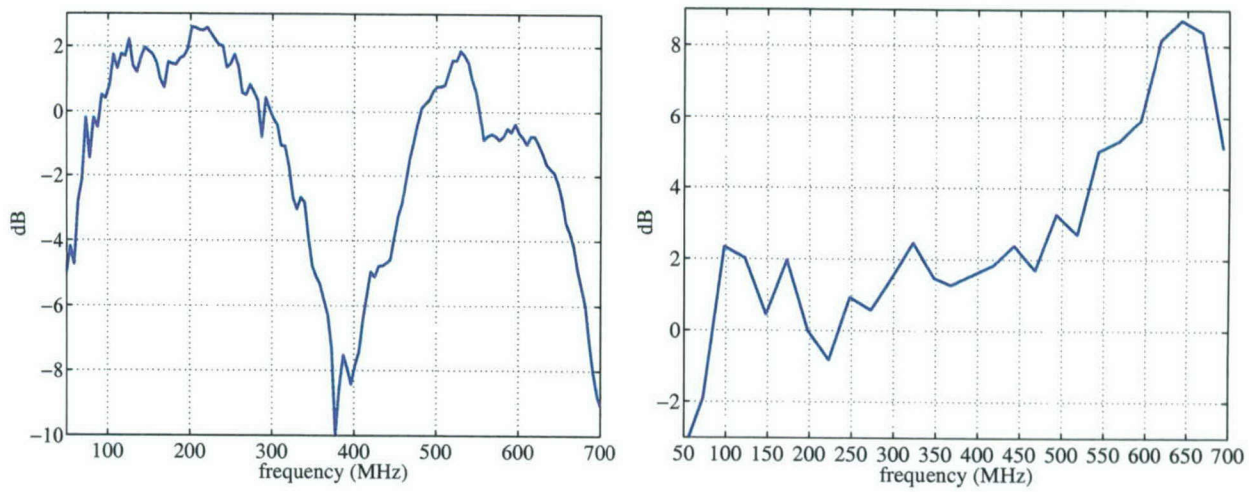

(a) Biconical receive antenna

(b) Transmit array

Fig. 9. Measured boresight gain vs. frequency of the receive and transmit antenna.

we will use a much larger ground plane. Fig. 10(b) shows measured patterns for the whole array when uniformly driven (Σ beam) at various frequencies. Fig. 10(c) shows measured patterns for Σ beams at various frequencies, steered to 60°. We can see that the result is not a beam that peaks at 60°, but rather understeers by an amount that depends on the frequency. This agrees with electromagnetic simulations which confirm that this is a consequence of the small ground plane. Somewhat unexpectedly, the effect on a Δ beam is to overscan, as shown in Fig. 10(c) for three beams nominally steered to $-15°$, 0°, and 15°. Finally, Figs. 10(e) and 10(f) demonstrate the versatility of a fully digital transmit array, each showing seven simultaneously transmitted beams across a wide range of frequencies in both the first and second Nyquist zones.

C. Multichannel Modulation: Space-Time vs. Temporal-Only

Because of the previously discussed problems with measuring low-noise signals, all of the multichannel tests worth reporting used high-bandwidth $\Delta\Sigma$ waveforms which have relatively high noise floors. This allows us to draw some reasonably fair comparisons between conventional and spatio-temporal $\Delta\Sigma$ modulation. It also demonstrates that spatio-temporal $\Delta\Sigma$ modulation still functions as expected at low temporal oversampling ratios, where conventional $\Delta\Sigma$ largely fails.

To generate the spatio-temporal $\Delta\Sigma$ signals, a matrix loop filter was designed to minimize noise power from $-90°$ to 90° in a 200 MHz wide temporal frequency band centered at 200 MHz. A uniformly illuminated boresight beam at 201 MHz was then modulated using this filter. For comparison, a scalar loop filter of the same length was designed to minimize the noise power in the same temporal band. A 201 MHz sinusoid was then modulated six times, using randomized starting states and dither to ensure that the channels were uncorrelated. The measured array pattern and frequency response were used to simulate the system. The simulated and measured power spectra for both cases are shown in Figs. 11(a) through 11(d). The resulting SNR across the 200 MHz band is shown in Fig. 11(e) as a function of angle. In both cases the measured SNR at boresight is a relatively good match to the simulated SNR, but the former falls off much more quickly with angle. This is because the simulations expect the noise and signal to both fall off as the array pattern. That the measured noise does not fall off appreciably indicates that, at least at higher angles, it is largely interference rather than expected $\Delta\Sigma$ quantization noise. Further reinforcing this is that the noise power spectra for both cases are very similar, and show components not present in the simulation. Even with this interference, at boresight the spatio-temporal modulated signal shows an 8 dB SNR improvement over the conventional modulator.

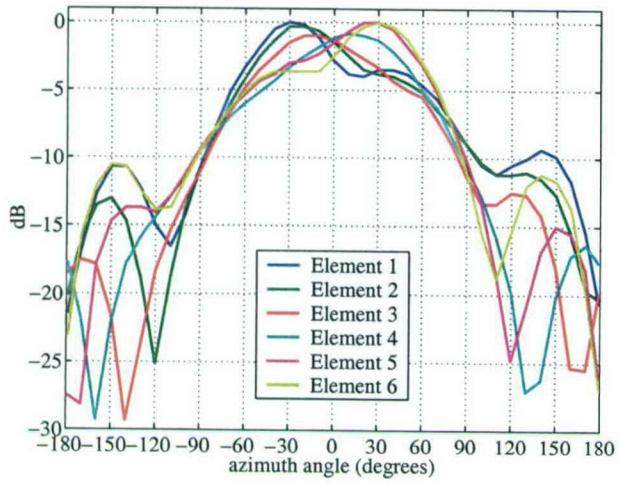

(a) Element patterns at 200 MHz

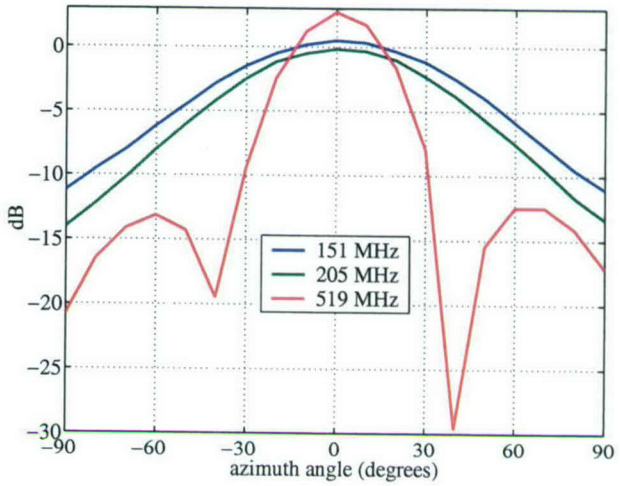

(b) Boresight Σ array patterns

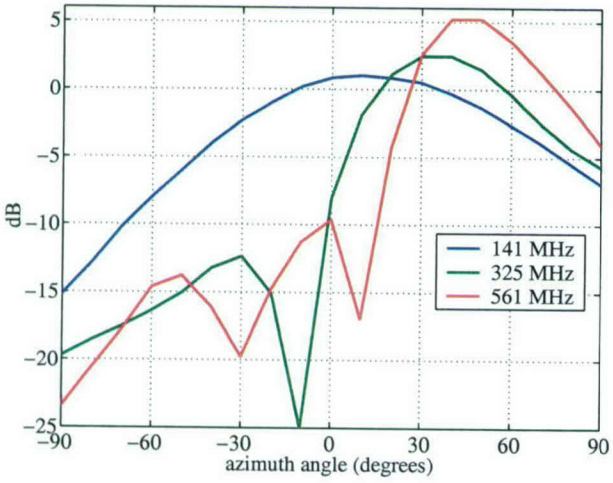

(c) Σ array patterns scanned to 60°

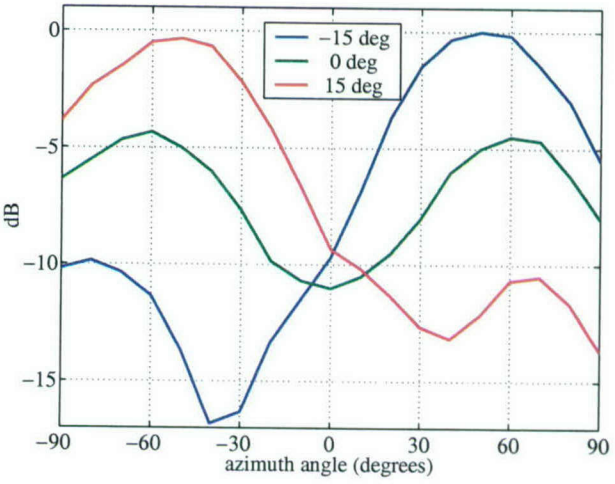

(d) Scanned Δ patterns at 200 MHz

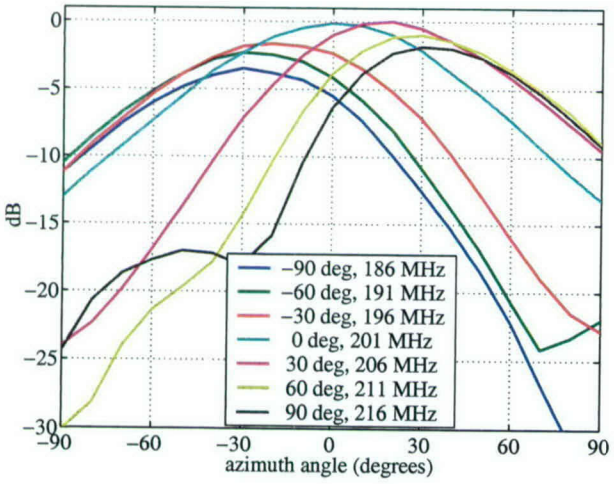

(e) Seven simultaneous beams, first Nyquist band

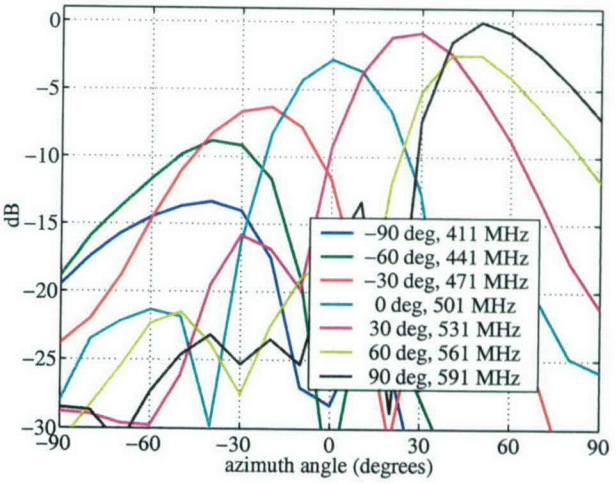

(f) Seven simultaneous beams, second Nyquist band

Fig. 10. Various measured array patterns.

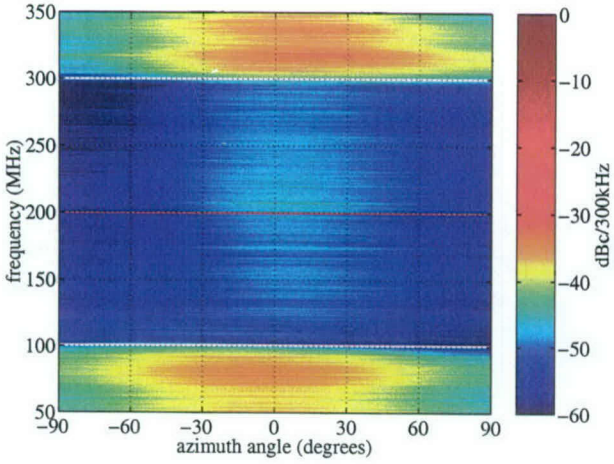

(a) Simulated spatio-temporal $\Delta\Sigma$ power spectrum

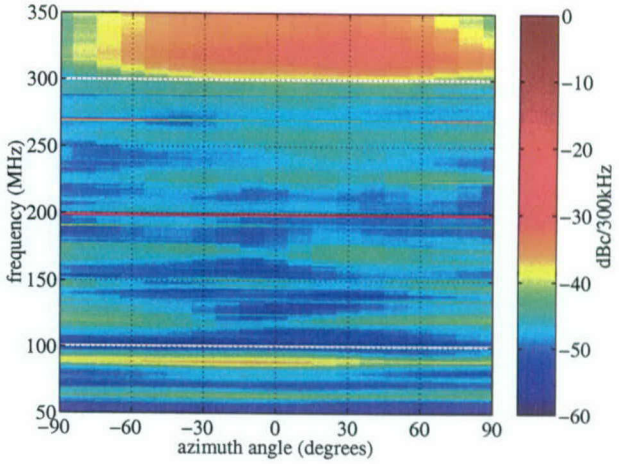

(b) Measured spatio-temporal $\Delta\Sigma$ power spectrum

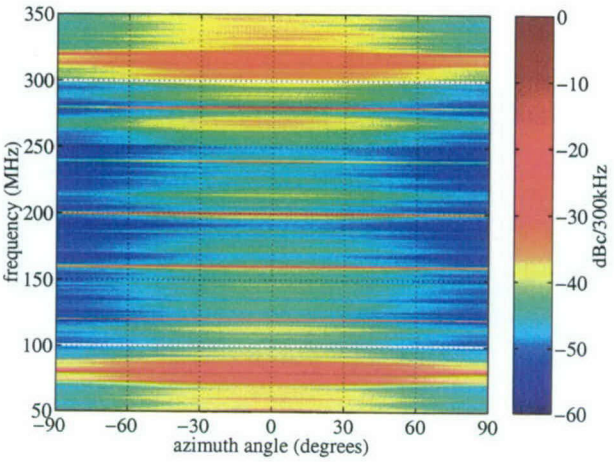

(c) Simulated temporal-only $\Delta\Sigma$ power spectrum

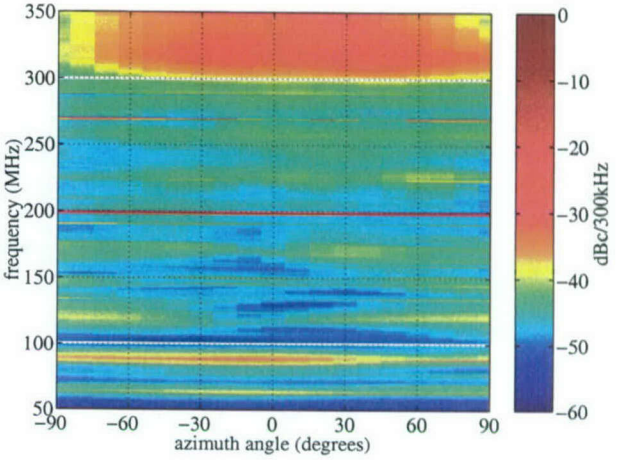

(d) Measured temporal-only $\Delta\Sigma$ power spectrum

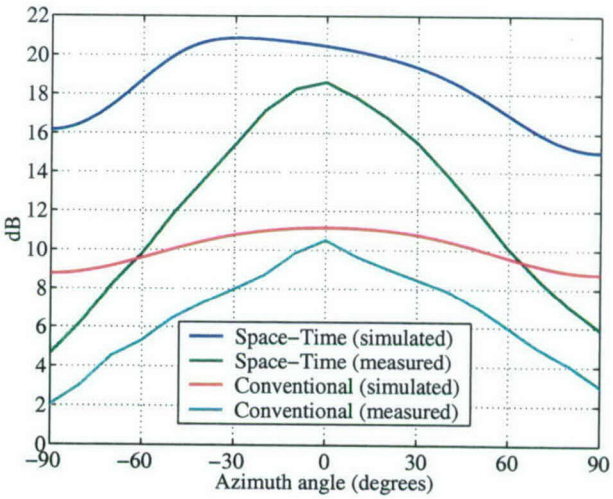

(e) SNR vs. angle

Fig. 11. Simulated and measured power spectra for spatio-temporal and conventional temporal-only $\Delta\Sigma$ modulation of a 201 MHz sinusoid within a 200 MHz wide noise notch.

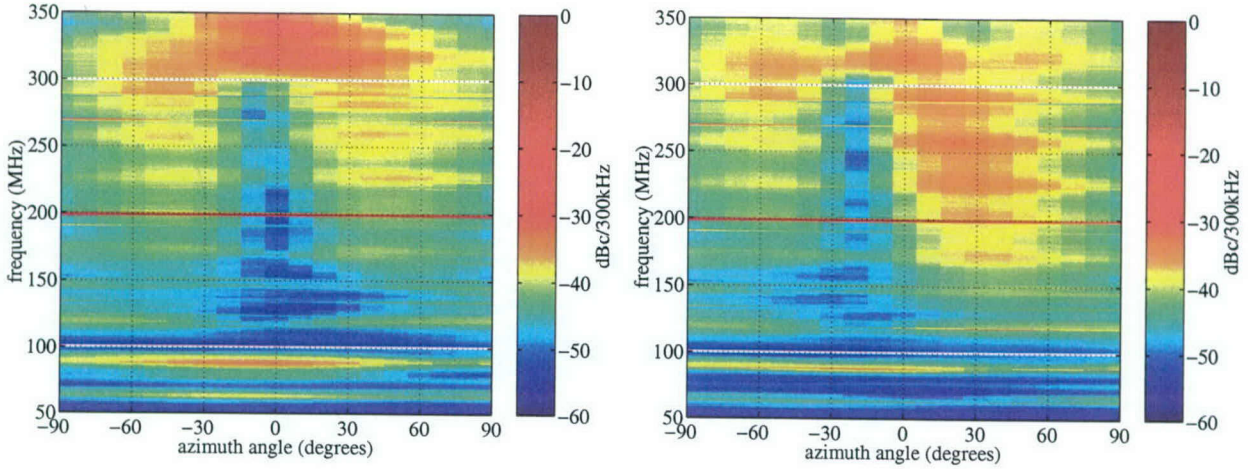

(a) Boresight noise notch

(b) $-30°$ noise notch

Fig. 12. Power spectra of received spatio-temporal $\Delta\Sigma$-modulated signal with a noise notch at a single frequency.

D. Illustrating Spatial Noise Shaping

In the previous tests, and in most practical systems, we wish to suppress in-band quantization noise for all visible angles. It is useful for illustrative purposes, however, to design a loop filter that only minimizes quantization noise at a single angle. This results in the same visual effect as is provided by the temporal frequency notch in an unfiltered modulator output. This was done for both boresight and $-30°$, with the received power spectra shown in Fig. 12. Some of the same understeering effect as before can be seen. Although it is difficult to produce a narrow notch with just six elements, it is clearly visible in both plots. These figures also demonstrate that we are not simply nesting a 1D spatial $\Delta\Sigma$ modulator inside a 1D temporal $\Delta\Sigma$ modulator, as others have done. Had we done so, the noise notch would extend out to all frequencies, albeit not as deep as where it intersected with the 200 MHz temporal frequency notch. Here it "dead ends" at the temporal frequency band edges.

IV. Conclusions

The explicit goal of these experiments was to verify that spatio-temporal quantization noise could be shaped through feedback to provide greater SNR than with temporal noise shaping alone, and to show how a spatio-temporally oversampled array using simply binary drivers and noise shaping could be digitally controlled. This was accomplished, albeit with extremely unspectacular performance. However, the most important lesson to be learned from these experiments is that clever signal processing can augment, but is no substitute for, proper RF electronics design. The requirements of a spatio-temporal delta-sigma array are sufficiently different from conventional RF systems that a concerted multiyear effort aimed at developing new driver topologies and driver-element integration will be needed before next-generation performance levels can be achieved.

References

[1] D. P. Scholnik and J. O. Coleman, "Space-time vector delta-sigma modulation," in *Proc. IEEE Int. Symp. Circuits and Systems*, Scottsdale, AZ, May 2002.

[2] D. P. Scholnik and J. O. Coleman, "Computability constraints in space-time delta-sigma arrays," in *Proc. Asilomar Conf. on Signals, Systems, and Computers*, Pacific Grove, CA, Nov. 2001.

[3] D. P. Scholnik and J. O. Coleman, "Joint spatial and temporal delta-sigma modulation for wideband antenna arrays and video halftoning," in *Proc. IEEE Int. Conf. Acoustic, Speech, and Signal Processing*, Salt Lake City, UT, May 2001.